Direct evidence for a magnetic *f*-electron–mediated pairing mechanism of heavy-fermion superconductivity in $CeCoIn_5$

John S. Van Dyke[a], Freek Massee[b,c], Milan P. Allan[b,c,d], J. C. Séamus Davis[b,c,e,f,1], Cedomir Petrovic[b], and Dirk K. Morr[a,1]

[a]Department of Physics, University of Illinois at Chicago, Chicago, IL 60607; [b]Condensed Matter Physics and Materials Science Department, Brookhaven National Laboratory, Upton, NY 11973; [c]Laboratory of Atomic and Solid State Physics, Department of Physics, Cornell University, Ithaca, NY 14853; [d]Department of Physics, Eidgenössische Technische Hochschule Zürich, CH-8093 Zurich, Switzerland; [e]School of Physics and Astronomy, University of St. Andrews, Fife KY16 9SS, United Kingdom; and [f]Kavli Institute at Cornell, Cornell University, Ithaca, NY 14853

Contributed by J. C. Séamus Davis, May 21, 2014 (sent for review April 23, 2014; reviewed by Zachary Fisk and Andrey Chubukov)

To identify the microscopic mechanism of heavy-fermion Cooper pairing is an unresolved challenge in quantum matter studies; it may also relate closely to finding the pairing mechanism of high-temperature superconductivity. Magnetically mediated Cooper pairing has long been the conjectured basis of heavy-fermion superconductivity but no direct verification of this hypothesis was achievable. Here, we use a novel approach based on precision measurements of the heavy-fermion band structure using quasiparticle interference imaging to reveal quantitatively the momentum space (*k*-space) structure of the *f*-electron magnetic interactions of $CeCoIn_5$. Then, by solving the superconducting gap equations on the two heavy-fermion bands $E_{\boldsymbol{k}}^{\alpha,\beta}$ with these magnetic interactions as mediators of the Cooper pairing, we derive a series of quantitative predictions about the superconductive state. The agreement found between these diverse predictions and the measured characteristics of superconducting $CeCoIn_5$ then provides direct evidence that the heavy-fermion Cooper pairing is indeed mediated by *f*-electron magnetism.

heavy fermion materials | unconventional superconductivity | *f*-electron–mediated pairing mechanism

Superconductivity of heavy fermions is of abiding interest, both in its own right (1–7) and because it could exemplify the unconventional Cooper pairing mechanism of high-temperature superconductors (8–11). Heavy-fermion compounds are intermetallics containing magnetic ions in the 4*f*- or 5*f*-electronic state within each unit cell. At high temperatures, each *f*-electron is localized at a magnetic ion (Fig. 1*A*). At low temperatures, interactions between *f*-electron spins (red arrows Fig. 1*A*) lead to the formation of a narrow but the subtly curved *f*-electron band $\varepsilon_{\boldsymbol{k}}^{f}$ near the chemical potential (red curve, Fig. 1*B*), and Kondo screening hybridizes this band with the conventional *c*-electron band $\varepsilon_{\boldsymbol{k}}^{c}$ of the metal (black curve, Fig. 1*B*). As a result, two new heavy-fermion bands $E_{\boldsymbol{k}}^{\alpha,\beta}$ (Fig. 1*C*) appear within a few millielectron volts of the Fermi energy. Their electronic structure is controlled by the hybridization matrix element $s_{\boldsymbol{k}}$ for interconversion of conduction *c*-electrons to *f*-electrons and vice-versa, such that

$$E_{\boldsymbol{k}}^{\alpha,\beta}=\frac{\varepsilon_{\boldsymbol{k}}^{c}+\varepsilon_{\boldsymbol{k}}^{f}}{2}\pm\sqrt{\left(\frac{\varepsilon_{\boldsymbol{k}}^{c}-\varepsilon_{\boldsymbol{k}}^{f}}{2}\right)^{2}+s_{\boldsymbol{k}}^{2}}. \qquad [1]$$

The momentum structure of the narrow bands of hybridized electronic states (Eq. **1** and Fig. 1*C*, blue curves at left) near the Fermi surface then directly reflects the form of magnetic interactions encoded within the parent *f*-electron band $\varepsilon_{\boldsymbol{k}}^{f}$. It is these interactions that are conjectured to drive the Cooper pairing (1–5) and thus the opening up of a superconducting energy gap (Fig. 1*C*, yellow curves at right).

Heavy Fermions and Cooper Pairing

Theoretical studies of the microscopic mechanism sustaining the Cooper pairing of such heavy fermions typically consider the electronic fluid as a Fermi liquid but with strong antiferromagnetic spin fluctuations derived from the *f*-electron magnetism. Moreover, it has been long hypothesized that it is these spin fluctuations that generate the attractive Cooper pairing interaction in heavy-fermion materials, specifically, in the *d*-wave channel (1–7). Why, in the decades since heavy-fermion superconductivity was discovered (12), has this been so extremely difficult to prove? The crux is that identification of the pairing mechanism in a heavy-fermion compound requires two specific pieces of information: the heavy-band structures $E_{\boldsymbol{k}}^{\alpha,\beta}$ and the *k*-space structure of the superconducting gaps $\Delta_{\boldsymbol{k}}^{\alpha,\beta}$ (which encode the essentials of the pairing process). However, determination of the characteristic heavy-fermion band structure requires precision measurement of $E_{\boldsymbol{k}}^{\alpha,\beta}$ both above and below the Fermi energy (Fig. 1*B*), making it problematic for angle-resolved photoemission. Moreover, due to the extreme flatness of the heavy bands $\left|dE_{\boldsymbol{k}}^{\alpha,\beta}/dk\right|\to 0$ and a maximum superconducting gap of typically only a few hundred microelectron volts, no techniques existed with sufficient combined energy resolution $\delta E\leq 100$ μeV and *k*-space resolution to directly measure $E_{\boldsymbol{k}}^{\alpha,\beta}$ and $\Delta_{\boldsymbol{k}}^{\alpha,\beta}$ for any heavy-fermion superconductor. Unambiguous identification of the Cooper pairing mechanism had therefore proven impossible.

Heavy-Fermion Quasiparticle Interference: Experiment and Theory

Very recently, however, this situation has changed (13–15). Heavy-fermion Bogoliubov quasiparticle interference (BQPI) imaging

Significance

In heavy-fermion materials, the magnetic moment of an *f*-electron atom, such as Ce, is screened via the Kondo effect resulting in the splitting of a conventional light band into two heavy bands within few millielectron volts of the Fermi energy. For decades it has been hypothesized that Cooper pairing and superconductivity of the resulting heavy electrons are mediated by the *f*-electron magnetism. By extracting the magnetic interactions of $CeCoIn_5$ from heavy-fermion scattering interference, and by then predicting quantitatively a variety of characteristics expected for unconventional superconductivity driven by them, we provide direct evidence that the heavy-fermion Cooper pairing in this material is indeed mediated by *f*-electron magnetism.

Author contributions: J.C.S.D. and D.K.M. designed research; J.S.V., F.M., M.P.A., C.P., and D.K.M. performed research; C.P. synthesized the samples; J.S.V., F.M., and D.K.M. analyzed data; and J.S.V., F.M., J.C.S.D., and D.K.M. wrote the paper.

Reviewers: Z.F., University of California, Irvine; and A.C., University of Wisconsin.

The authors declare no conflict of interest.

[1]To whom correspondence may be addressed. Email: jcseamusdavis@gmail.com or dkmorr@uic.edu.

This article contains supporting information online at www.pnas.org/lookup/suppl/doi:10.1073/pnas.1409444111/-/DCSupplemental.

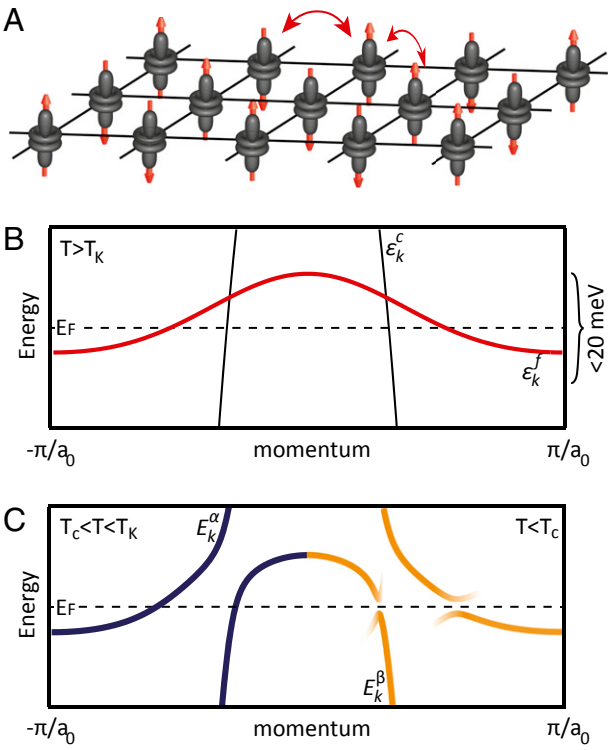

Fig. 1. Effects of *f*-electron magnetism in a heavy-fermion material. (*A*) The magnetic subsystem of $CeCoIn_5$ consists of almost localized magnetic *f*-electrons (red arrows) with a weak hopping matrix element yielding a very narrow band with strong magnetic interactions between the *f*-electron spins. (*B*) The heavy *f*-electron band is shown schematically in red and the light *c*-electron band in black. (*C*) On the left, schematic of the result of hybridizing the *c*- and *f*-electrons in *B* into new composite electronic states referred to as heavy fermions (blue). On the right, the opening of a superconducting energy gap is schematically shown by back-bending bands near the chemical potential. The microscopic interactions driving Cooper pairing of these states, and thus of heavy-fermion superconductivity, have not been identified unambiguously for any heavy-fermion compound.

implemented with $\delta E \approx 75$ μeV at $T \leq 250$ mK allowed detailed measurements of the $\boldsymbol{k}$-space energy gap structure $\Delta_{\boldsymbol{k}}^{\alpha,\beta}$ for the archetypical heavy-fermion superconductor $CeCoIn_5$ (16). Its normal-state properties are somewhat unconventional (17, 18) and seem to reflect the presence of strong antiferromagnetic spin fluctuations (19) [whether these fluctuations are associated with the existence of a true quantum critical point (20–22) is presently unclear]. The compound is electronically quasi-2D (23) and its $T_c = 2.3$ K is among the highest of the heavy-fermion superconductors (16). The Cooper pairs are spin singlets (24, 25) and therefore $\Delta_{\boldsymbol{k}}^{\alpha,\beta}$ must exhibit even parity. Application of the recently developed heavy-fermion QPI imaging technique (13, 15) to $CeCoIn_5$ reveals the expected development with falling temperature of the heavy bands (26) in agreement with angle-resolved photoemission (27, 28). Evidence for a spin fluctuation-driven pairing mechanism in related heavy fermion compounds was adduced by comparing the change in the magnetic exchange energy to the condensation energy (29). At lower temperatures, there is clear evidence that $CeCoIn_5$ is an unconventional superconductor with a nodal energy gap (30–33) possibly with $d_{x^2-y^2}$ order parameter symmetry (15, 34) [although this has not been verified directly using a phase-sensitive method (35)]. The microscopic Cooper pairing mechanism of $CeCoIn_5$ has, however, not been established (7,16, 25, 36).

Heavy QPI imaging and BQPI studies of $CeCoIn_5$ at ~ 250 mK can now yield accurate knowledge of the $\boldsymbol{k}$-space structure of both $E_{\boldsymbol{k}}^{\alpha,\beta}$ and $\Delta_{\boldsymbol{k}}^{\alpha,\beta}$ (15). Using a He-3 refrigerator-based spectroscopic imaging scanning tunneling microscopy system operating down to an electron temperature of 250 mK, we image the differential conductance $g(\boldsymbol{r},E)$ with atomic resolution and register, and then determine $g(\boldsymbol{q},E)$, the power spectral density Fourier transform of each image. Recently, it was demonstrated that this approach can be used to identify elements of heavy-fermion $\boldsymbol{k}$-space electronic structure (13, 37) because elastic scattering of electrons from $-\boldsymbol{k}(E)$ to $+\boldsymbol{k}(E)$ generates density-of-states interference patterns occurring as maxima at $\boldsymbol{q}(E) = \boldsymbol{k}(E) - (-\boldsymbol{k}(E)) = 2\boldsymbol{k}(E)$ in $g(\boldsymbol{q},E)$. The onset of the heavy bands in $CeCoIn_5$ is then detected (15) as a sudden transformation of the slowly changing structure of $g(\boldsymbol{q},E)$, which appears at $E \approx 4$ meV, followed by a rapid evolution of the maximum intensity features toward a smaller $|\boldsymbol{q}|$-radius, then by an abrupt jump to a larger $|\boldsymbol{q}|$-radius, and then by a second rapid diminution of interference pattern $|\boldsymbol{q}|$-radii. Thus, heavy-fermion QPI directly reveals the momentum structure of two heavy bands in the energy range -4 meV $< E < 12$ meV, and the formation of their hybridization gap. Fig. 2 *A* and *B* shows typical examples of our $CeCoIn_5$ heavy-fermion QPI data and shows the comparison of measured $g(\boldsymbol{q},E)$ and predicted $g(\boldsymbol{q},E)$ derived from our precision model for the $E_{\boldsymbol{k}}^{\alpha,\beta}$ (*SI Text*, section 1.2). The Fermi surface deduced from these measurements is shown in Fig. 2*C*, and consists of a small hole-like Fermi surface arising from the heavy β-band and two larger electron-like Fermi surfaces (α_1, α_2) resulting from the heavy α-band (15) (*SI Text*, section 1). Eq. **1**

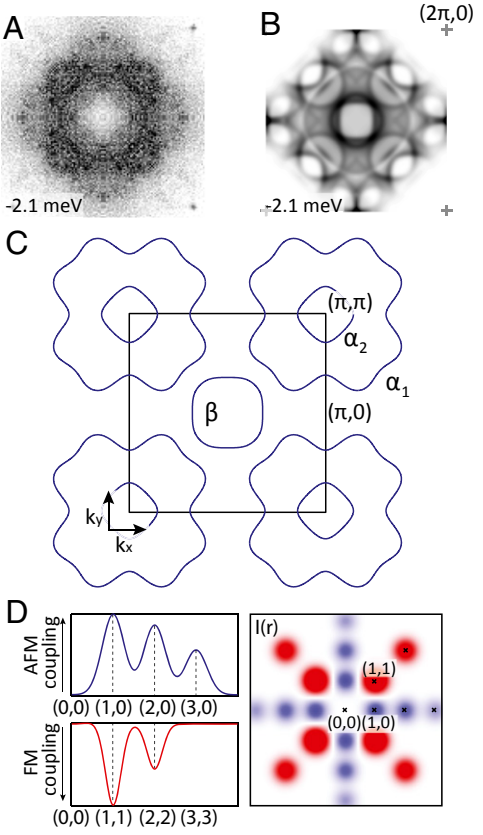

Fig. 2. Heavy-fermion band-structure determination for $CeCoIn_5$. (*A*) Typical example of measured $g(\boldsymbol{q},E)$ within the heavy bands. (*B*) Typical example of predicted $g(\boldsymbol{q},E)$ for our parameterization of the heavy-band structure. They are in good detailed agreement, as are the equivalent pairs of measured and predicted $g(\boldsymbol{q},E)$ (*SI Text*, section 1). (*C*) The Fermi surface of our heavy-band structure model (*SI Text*, section 1). (*D*) *r*-space structure of the magnetic interaction strength, $I(\boldsymbol{r})$, as obtained from Eq. **S2b**. This form of $I(\boldsymbol{r})$ reflects the existence of strong antiferromagnetic (AFM) correlations between adjacent localized moments and ferromagnetic (FM) correlations between next nearest neighbors.

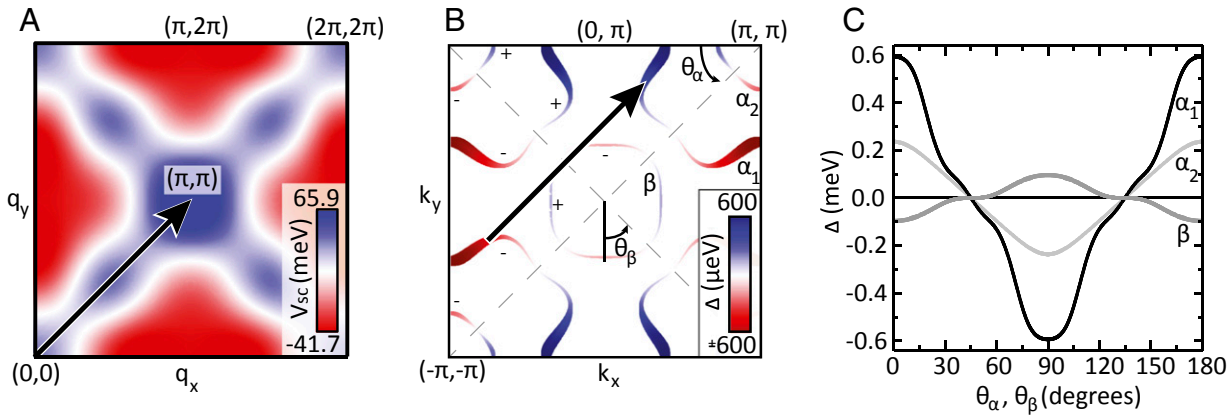

Fig. 3. Predicted gap structure for $CeCoIn_5$ if *f*-electron magnetism mediates Cooper pairing. (*A*) Magnetically mediated pairing potential, $V_{SC}(\boldsymbol{q}) = -I(\boldsymbol{q})/2$, of $CeCoIn_5$. The arrow represents the momentum $\boldsymbol{Q} = (\pm 1, \pm 1)\pi/a_0$, where the pairing potential is large and repulsive. (*B*) Angular dependence of the predicted superconducting gaps $\Delta_{\boldsymbol{k}}^{\alpha,\beta}$ in the α- and β-bands (note that the angles θ_α and θ_β are measured around $\boldsymbol{q} = (\pi,\pi)$ and $\boldsymbol{q} = (0,0)$, respectively). The thickness and color of the Fermi surface encode the superconducting energy gap size and sign, respectively. These results were obtained at $T = 0$ using a Debye frequency of $\omega_D = 0.66$ meV. The arrow represents the momentum $\boldsymbol{Q} = (\pm 1, \pm 1)\pi/a_0$ which connects momentum states on the Fermi surfaces where the superconducting gaps possess different signs. (*C*) Predicted values of the superconducting energy gaps as a function of the Fermi surface angle. The largest gap is located on the α_1-Fermi surface, whereas a small gap exists on the central β–Fermi surface and the outer α_2-Fermi surface.

shows how the precise dispersions $E_{\boldsymbol{k}}^{\alpha,\beta}$ of the two heavy-fermion bands are fixed by $\varepsilon_{\boldsymbol{k}}^{f}$, which is itself generated by the Heisenberg interaction energy $I(\boldsymbol{r}-\boldsymbol{r}')\boldsymbol{S}_{\boldsymbol{r}}\cdot\boldsymbol{S}_{\boldsymbol{r}'}$ between spins $\boldsymbol{S}_{\boldsymbol{r}}$ and $\boldsymbol{S}_{\boldsymbol{r}'}$ at *f*-electron sites $\boldsymbol{r}$ and $\boldsymbol{r}'$ (38) (Eq. **S1** and *SI Text*, section 1). Therefore, the real space ($\boldsymbol{r}$-space) form of the magnetic interaction potential, $I(\boldsymbol{r}-\boldsymbol{r}')$, can be determined directly from the measured $E_{\boldsymbol{k}}^{\alpha,\beta}$ (Eq. **S2b** and *SI Text*, section 1). Carrying out this procedure reveals quantitatively the form of $I(\boldsymbol{r})$ for the *f*-electron magnetic interactions of $CeCoIn_5$ (Fig. 2*D*) and therefore that strong antiferromagnetic interactions occur between adjacent *f*-electron moments (*SI Text*, section 1).

Solution of Gap Equations with a Magnetic *f*-Electron Interaction Kernel

These interactions are hypothesized to give rise to an effective electron-pairing potential $V_{SC}(\boldsymbol{r}-\boldsymbol{r}') = -I(\boldsymbol{r}-\boldsymbol{r}')/2$ (Eq. **S14** and *SI Text*, section 2.1), with the opposite sign to $I(\boldsymbol{r}-\boldsymbol{r}')$ because antiparallel spins at sites $\boldsymbol{r}$ and $\boldsymbol{r}'$ (for $I > 0$) experience an attractive ($V_{SC} < 0$) pairing potential; we are assuming spin-singlet pairing throughout. Fourier transformation of $V_{SC}(\boldsymbol{r})$ yields $V_{SC}(\boldsymbol{q})$ as shown in Fig. 3*A*, thereby revealing that the putative pairing potential $V_{SC}(\boldsymbol{q})$ is strongly repulsive at $\boldsymbol{q} = (\pm 1, \pm 1)\pi/a_0$ and attractive at $\boldsymbol{q} = (\pm 1, 0)\pi/a_0$; $(0, \pm 1)\pi/a_0$. It is this strong repulsion at $\boldsymbol{q} = (\pm 1, \pm 1)\pi/a_0$ which is the long-anticipated (1–11) requirement for unconventional Cooper pairing to be mediated by antiferromagnetic interactions. Finally, inserting this hypothesized pairing potential $V_{SC}(\boldsymbol{q})$ into the coupled superconducting gap equations for both heavy bands $E_{\boldsymbol{k}}^{\alpha,\beta}$ of $CeCoIn_5$ yields

$$\Delta_{\boldsymbol{k}}^{\alpha} = -\frac{x_{\boldsymbol{k}}^2}{N}\sum_{\boldsymbol{p}}{}' V_{SC}(\boldsymbol{p}-\boldsymbol{k}) \times\left[x_{\boldsymbol{p}}^2\frac{\Delta_{\boldsymbol{p}}^{\alpha}}{2\Omega_{\boldsymbol{p}}^{\alpha}}\tanh\left(\frac{\Omega_{\boldsymbol{p}}^{\alpha}}{2k_BT}\right)+w_{\boldsymbol{p}}^2\frac{\Delta_{\boldsymbol{p}}^{\beta}}{2\Omega_{\boldsymbol{p}}^{\beta}}\tanh\left(\frac{\Omega_{\boldsymbol{p}}^{\beta}}{2k_BT}\right)\right]$$

$$\Delta_{\boldsymbol{k}}^{\beta} = -\frac{w_{\boldsymbol{k}}^2}{N}\sum_{\boldsymbol{p}}{}' V_{SC}(\boldsymbol{p}-\boldsymbol{k}) \times\left[x_{\boldsymbol{p}}^2\frac{\Delta_{\boldsymbol{p}}^{\alpha}}{2\Omega_{\boldsymbol{p}}^{\alpha}}\tanh\left(\frac{\Omega_{\boldsymbol{p}}^{\alpha}}{2k_BT}\right)+w_{\boldsymbol{p}}^2\frac{\Delta_{\boldsymbol{p}}^{\beta}}{2\Omega_{\boldsymbol{p}}^{\beta}}\tanh\left(\frac{\Omega_{\boldsymbol{p}}^{\beta}}{2k_BT}\right)\right]. \quad [2]$$

Here $\Omega_{\boldsymbol{p}}^{\alpha,\beta} = \sqrt{(E_{\boldsymbol{p}}^{\alpha,\beta})^2 + (\Delta_{\boldsymbol{p}}^{\alpha,\beta})^2}$ are the two pairs of Bogoliubov bands, $w_{\boldsymbol{k}}$ and $x_{\boldsymbol{k}}$, are the coherence factors of the heavy-fermion hybridization process, and the primed sum runs only over those momentum states $\boldsymbol{p}$ whose energies $E_{\boldsymbol{p}}^{\alpha,\beta}$ lie within the interaction cutoff energy, ω_D, of the Fermi energy. Our solutions to Eq. **2** (*SI Text*, section 2) predict that the α- and β-bands of $CeCoIn_5$ possess superconducting gaps $\Delta_{\boldsymbol{k}}^{\alpha,\beta}$ of nodal $d_{x^2-y^2}$ symmetry as shown in Fig. 3 *B* and *C*. This symmetry is dictated by the large repulsive pairing potential near $\boldsymbol{Q} = (\pm 1, \pm 1)\pi/a_0$ (arrow in Fig. 3*A*), which requires that the superconducting gap changes sign between Fermi surface points connected by $\boldsymbol{Q}$, as shown in Fig. 3*B*. We predict that the maximum gap value occurs on the α_1-Fermi surface, with $\Delta_{\boldsymbol{k}}^{\alpha,\beta}$ being well approximated by

$$\Delta_{\boldsymbol{k}}^{\alpha} = \frac{\Delta_0^{\alpha}}{2}\left\{\left[\cos(k_x)-\cos(k_y)\right]+\alpha_1\left[\cos(2k_x)-\cos(2k_y)\right] + \alpha_2\left[\cos(3k_x)-\cos(3k_y)\right]\right\} \quad [3]$$

$$\Delta_{\boldsymbol{k}}^{\beta} = \frac{\Delta_0^{\beta}}{2}\left[\cos(k_x)-\cos(k_y)\right]^3.$$

Here $\Delta_0^{\alpha} = 0.49$ meV, $\alpha_1 = -0.61$, $\alpha_2 = -0.08$, and $\Delta_0^{\beta} = -1.04$ meV represent the quantitative predictions for the $\Delta_{\boldsymbol{k}}^{\alpha,\beta}$ in Eq. **3** derived from the hypothesis of Eq. **2** with $\omega_D = 0.66$ meV constraining the maximum possible energy gap to be $\Delta_{max} \leq 600$ μeV. The solution of Eq. **2** (without any further adjustable parameters) then also predicts $T_c = 2.96$ K, which is reduced to $T_c = 2.55$ K once one accounts for the experimentally observed mean free path of $l = 81$ nm (Eq. **S21**). Overall, the predicted gap structure $\Delta_{\boldsymbol{k}}^{\alpha,\beta}$ (Eq. **3**) and T_c are in striking quantitative agreement with the measured $\Delta_i(\boldsymbol{k})$ (15) and $T_c = 2.3$ K (16) for $CeCoIn_5$.

These results raise several interesting questions. First, although ω_D appears above as a phenomenological parameter, the question naturally arises of how such a cross-over scale arises from the interplay between the form of the spin excitation spectrum, the strength of the coupling between *f*-electrons and spin fluctuations, and the flatness of the *f*-electron bands. To address this question, it will be necessary to extend the above method to a strong coupling, Eliashberg-type approach. Second, although our approach assumes that the formation of coherent (screened) Kondo lattice is concluded prior to the onset of superconductivity, it has been suggested (39) that singlet formation might continue into the

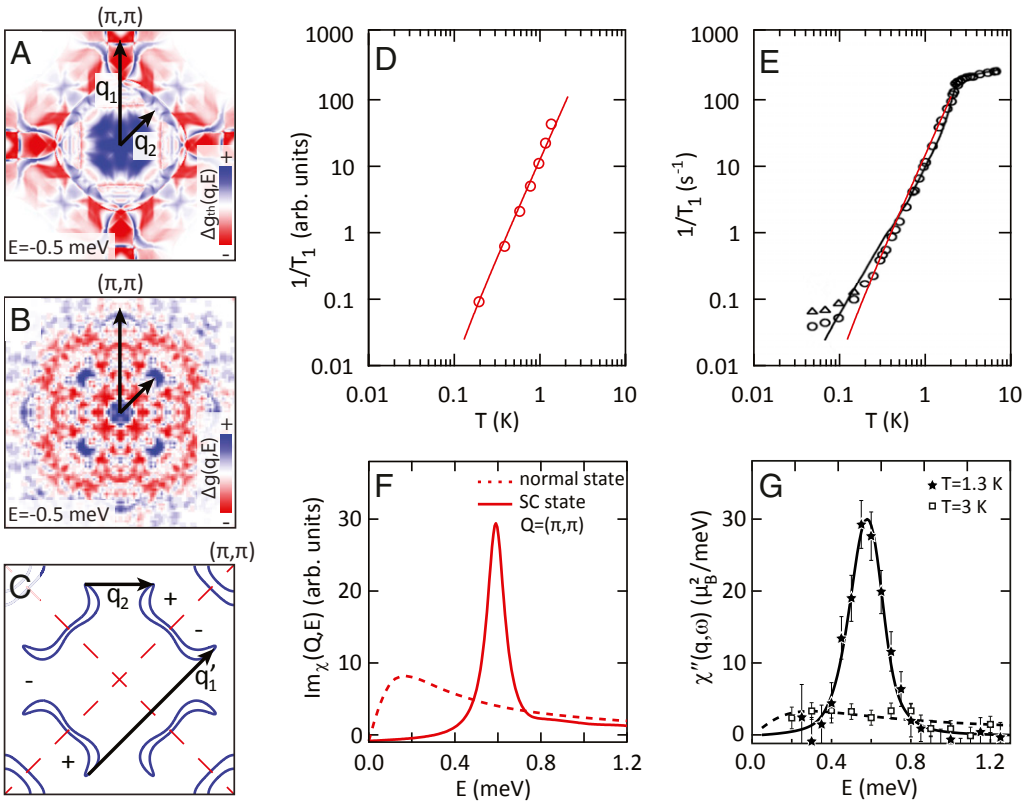

Fig. 4. Comparison of predicted phenomenology of $CeCoIn_5$ if *f*-electron magnetism mediates Cooper pairing, with experimental data. (*A*) Predicted PQPI scattering pattern for the predicted $\Delta_{\boldsymbol{k}}^{\alpha,\beta}$ with $d_{x^2-y^2}$ symmetry: $\Delta g(\boldsymbol{q},E,B)=g(\boldsymbol{q},E,B)-g(\boldsymbol{q},E,0)$ for $E=-0.5$ meV. $\Delta g(\boldsymbol{q},E,B)$ is negative (red) for scattering vectors connecting parts of the Fermi surface with opposite signs in the order parameter, such as $\boldsymbol{q}_1$ (*C*), whereas sign-preserving scattering leads to a positive $\Delta g(\boldsymbol{q},E,B)$ (blue) such as $\boldsymbol{q}_2$ (*C*). See *SI Text*, section 2.3 for full details. (*B*) Measured PQPI $\Delta g(\boldsymbol{q},E,B)=g(\boldsymbol{q},E,B)-g(\boldsymbol{q},E,0)$ for $E=-0.5$ meV. $g(\boldsymbol{q},E,B)$ and $g(\boldsymbol{q},E,0)$ are measured in the identical field of view using identical measurement parameters at $B=0$ and $B=3T$. $\Delta g(\boldsymbol{q},E,B)$ exhibits the same enhancement and suppression for $\boldsymbol{q}_{1,2}$ as in *A*. The good correspondence, especially for the relevant scattering vectors between regions whose gaps are predicted to have opposite signs between theoretically predicted $\Delta g(\boldsymbol{q},E,B)$ and measurements thereof is a phase-sensitive verification of a *d*-wave gap symmetry in $CeCoIn_5$. See *SI Text*, section 2.3 for additional energies and details. (*C*) Equal energy contour (EEC) for $E=-0.5$ meV used in *A* and *B* (i.e., momentum points with $E=-\Omega_{\boldsymbol{k}}^{\alpha\beta}$) in the superconducting state. Scattering processes yielding the dominant contribution to $g(\boldsymbol{q}_{1,2},E)$, with $\boldsymbol{q}_1(\boldsymbol{q}_2)$ connecting points on the EEC with opposite phases (the same phase) of the superconducting gap are shown (the phases are indicated by +/–). For simplicity, we show $\boldsymbol{q}_1'=(2\pi,2\pi)-\boldsymbol{q}_1$, the Umklapp vector to $\boldsymbol{q}_1$. Note that the coordinate system is rotated by 45° with respect to *A* and *B*. (*D*) Predicted temperature dependence of the nuclear relaxation rate $1/T_1$ for the superconducting state of $CeCoIn_5$ based on combining the *f*-electron magnetic interactions $I(\boldsymbol{q})$ and the predicted $\Delta_{\boldsymbol{k}}^{\alpha,\beta}$. (*E*) Measured temperature dependence of $1/T_1$ for the superconducting state of $CeCoIn_5$ (data from ref. 25). (*F*) Predicted imaginary part of the dynamical spin susceptibility $\chi(\boldsymbol{Q},E)$ at $\boldsymbol{Q}=(\pm1,\pm1)\pi/a_0$ in the superconducting state of $CeCoIn_5$ based on combining the *f*-electron magnetic interactions $I(\boldsymbol{q})$ and the predicted $\Delta_{\boldsymbol{k}}^{\alpha,\beta}$. A strong resonance is predicted below T_c at $E\approx0.6$ meV. (*G*) Measured imaginary part of the dynamical spin susceptibility $\chi(\boldsymbol{Q},E)$ at $\boldsymbol{Q}\approx(\pm1,\pm1)\pi/a_0$ in the superconducting state of $CeCoIn_5$ (modified from ref. 36). There is a strong quantitative correspondence to the model prediction.

superconducting state. New theoretical/experimental approaches will be required to determine if this type of composite pairing might be detectable in the temperature dependence of physical properties for $T\lesssim T_c$. Notwithstanding these questions, our first focus is now to evaluate the predictive utility of the relatively simple approach that was proposed originally (1–4) and has been implemented here.

Phase-Sensitive QPI

Given this detailed new understanding of $\Delta_{\boldsymbol{k}}^{\alpha,\beta}$ (Eq. **3** and Fig. 3 *B* and *C*), a variety of other testable predictions for superconducting characteristics of $CeCoIn_5$ become possible. In particular, the phase of the predicted $d_{x^2-y^2}$ symmetry gaps is directly reflected in the magnitude of $g(\boldsymbol{q},E)$. The scattering of Bogoliubov quasiparticles between momentum points $\boldsymbol{k}_1$ and $\boldsymbol{k}_2$ near the Fermi surface leads to a contribution to $g(\boldsymbol{q}=\boldsymbol{k}_1-\boldsymbol{k}_2,E)$ that is directly proportional to the product $\Delta_{\boldsymbol{k}_1}\Delta_{\boldsymbol{k}_2}$. For time-reversal invariant scalar-potential scattering, this contribution enters $g(\boldsymbol{q}=\boldsymbol{k}_1-\boldsymbol{k}_2,E)$ with a sign that is opposite to that for time-reversal violating magnetic scattering. As a result, changes in $g(\boldsymbol{q},E)$ generated by altering the nature of the scattering potential provide direct information on the relative phase difference between $\Delta_{\boldsymbol{k}_1}$ and $\Delta_{\boldsymbol{k}_2}$. This phenomenon has been beautifully demonstrated by considering magnetic field-induced changes in the conductance ratio in $Bi_2Sr_2CaCu_2O_8$, a single-band cuprate superconductor with $d_{x^2-y^2}$ symmetry (35). Although the predicted symmetry of $\Delta_{\boldsymbol{k}}^{\alpha,\beta}$ in $CeCoIn_5$ is similarly $d_{x^2-y^2}$ (Fig. 3), the detailed predictions for magnetic field-induced changes in $g(\boldsymbol{q},E)$ are quite complex because of the multiple superconducting gaps and intricate band geometry (*SI Text*, section 2.3). In Fig. 4*A* we show our predicted values of the field-induced QPI changes $\Delta g(\boldsymbol{q},E,B)=g(\boldsymbol{q},E,B)-g(\boldsymbol{q},E,0)$ for a typical energy, $E=-0.5$ meV below the gap maximum (*SI Text*, section 2.3). For comparison, in Fig. 4*B* we show the measured $\Delta g(\boldsymbol{q},E,B)$ at the same energy (*SI Text*, section 2.3). Not only is the agreement between them as to which regions of $\boldsymbol{q}$-space have enhanced or diminished scattering intensity evident, but they also demonstrate that $\Delta g(\boldsymbol{q},E,B)$ is positive (negative) for scattering vectors, $\boldsymbol{q}_1(\boldsymbol{q}_2)$ connecting parts of the Fermi surface with the same sign (different signs) of the superconducting gap (Fig. 4*C*). In contrast, the equivalent

predictions for phase-sensitive $\Delta g(\boldsymbol{q}, E, B)$ if the gap symmetry is a nodal s-wave bear little discernible relationship to the experimental data (*SI Text*, section 2.3). Thus, the application in $CeCoIn_5$ of the phase-sensitive QPI (PQPI) technique (35) reveals the predicted effects of sign changes in $d_{x^2-y^2}$ symmetry gaps of structure $\Delta_{\boldsymbol{k}}^{\alpha,\beta}$.

Spin Excitations

Lastly, by combining the f-electron magnetic interactions $I(\boldsymbol{r})$ (Fig. 2*D*) and the predicted $\Delta_{\boldsymbol{k}}^{\alpha,\beta}$ (Fig. 3), we can investigate the spin dynamics of $CeCoIn_5$ in the superconducting state (*SI Text*, section 3). One test for the nodal character of the predicted $d_{x^2-y^2}$ symmetry superconducting gap is the temperature dependence of the spin–lattice nuclear relaxation rate $1/T_1$: Its theoretically predicted form is shown in Fig. 4*D*. This is in good agreement with that of the measured $1/T_1$ reproduced in Fig. 4*E* from ref. 25. The theoretically predicted and experimentally observed power-law dependence $1/T_1 \approx T^{\alpha}$ with $\alpha \approx 2.5$ (straight lines in Fig. 4 *D* and *E*) shows an exponent that is reduced from the expected $\alpha = 3$ for a single-band $d_{x^2-y^2}$ wave superconductor. We demonstrate that this effect is actually due to fine details of the $\Delta_{\boldsymbol{k}}^{\alpha,\beta}$ multigap structure on the α- and β-Fermi surfaces (Fig. 3*C*). Finally, our theoretically predicted dynamic spin susceptibility in the superconducting state, using the extracted $I(\boldsymbol{r})$ and computed $\Delta_{\boldsymbol{k}}^{\alpha,\beta}$ with no further adjustable parameters, exhibits a spin resonance peak at $\boldsymbol{q} = (\pm 1, \pm 1)\pi/a_0$ and at $E \approx 0.6$ meV (*SI Text*, section 3) as shown in Fig. 4*F*. Such spin resonances are a direct signature of an unconventional superconducting order parameter: They arise from spin–flip transitions that involve states $\boldsymbol{k}_1$ and $\boldsymbol{k}_2$ with opposite signs of the superconducting gap. The experimental data on spin excitations in superconducting $CeCoIn_5$ from inelastic neutron scattering (reproduced from ref. 36) are shown in Fig. 4*G*, and exhibit a strong resonance located at $E \approx 0.6$ meV. The quantitative agreement between the predicted and measured energy of the spin resonance, as well as the form of the spin excitation spectrum both below and above T_c is remarkable. Moreover, the value of ω_D used in Eq. **2** is now seen to be quite consistent with the energy scale of the spin fluctuation spectrum (*SI Text*, section 4).

Conclusions

To summarize, the $\boldsymbol{r}$- and $\boldsymbol{q}$-space structure of magnetic interactions between f-electrons, $I(\boldsymbol{r})$ and $I(\boldsymbol{q})$, in the heavy-fermion state of $CeCoIn_5$ are determined quantitatively (Figs. 2*D* and 3*A*) from our measured heavy-band dispersions $E_{\boldsymbol{k}}^{\alpha,\beta}$ (*SI Text*, section 1). The coupled superconducting gap equations (Eq. **2**) are then solved using the hypothesis that it is these magnetic interactions that mediate Cooper pairing with $V_{SC}(\boldsymbol{q}) = -I(\boldsymbol{q})/2$. This allows a series of quantitative predictions regarding the physical properties of the superconducting state of $CeCoIn_5$. These include the superconducting critical temperature T_c, the $\boldsymbol{k}$-space structure of the two energy gaps $\Delta_{\boldsymbol{k}}^{\alpha,\beta}$ (Fig. 3), the phase-sensitive BQPI signature arising from the predicted $d_{x^2-y^2}$ symmetry of the superconducting gaps (Fig. 4*A*), the temperature dependence of the spin–lattice relaxation rate $1/T_1$ (Fig. 4*D*), and the existence and structure of a magnetic spin resonance near $\boldsymbol{q} = (\pm 1, \pm 1)\pi/a_0$ (Fig. 4*F*). The demonstrated quantitative agreement between all these predictions (themselves based on measured input parameters) and the disparate experimental characteristics of superconducting $CeCoIn_5$ (15, 16, 25, 29, 31, 34, 36) provide direct evidence that its Cooper pairing is indeed mediated by the residual f-electron magnetism (Eqs. **2** and **3**).

ACKNOWLEDGMENTS. We acknowledge and thank M. Aprili, P. Coleman, M. H. Fischer, R. Flint, P. Fulde, M. Hamidian, E.-A. Kim, D. H. Lee, A. P. Mackenzie, M. R. Norman, J. P. Reid, and J. Thompson for helpful discussions and communications. This work was supported by the US Department of Energy under Contract DEAC02-98CH10886 (to J.C.S.D. and C.P.) and Award DE-FG02-05ER46225 (to D.K.M. and J.S.V.).

1. Miyake K, Schmitt-Rink S, Varma CM (1986) Spin-fluctuation-mediated even-parity pairing in heavy-fermion superconductors. *Phys Rev B* 34(9):6554–6556.
2. Béal-Monod MT, Bourbonnais C, Emery VJ (1986) Possible superconductivity in nearly antiferromagnetic itinerant fermion systems. *Phys Rev B* 34(11):7716–7720.
3. Scalapino DJ, Loh E, Jr., Hirsch JE (1986) *d* -wave pairing near a spin-density-wave instability. *Phys Rev B* 34(11):8190–8192.
4. Scalapino DJ, Loh E, Jr., Hirsch JE (1987) Fermi-surface instabilities and superconducting *d*-wave pairing. *Phys Rev B* 35(13):6694–6698.
5. Lavagna M, Millis AJ, Lee PA (1987) *d* -wave superconductivity in the large-degeneracy limit of the Anderson lattice. *Phys Rev Lett* 58(3):266–269.
6. Coleman P, Andrei N (1989) Kondo-stabilised spin liquids and heavy-fermion superconductivity. *J Phys Condens Matter* 1(26):4057–4080.
7. Monthoux P, Lonzarich G (1999) *p*-wave and *d*-wave superconductivity in quasi-two-dimensional metals. *Phys Rev B* 59(22):14598–14605.
8. Monthoux P, Pines D, Lonzarich GG (2007) Superconductivity without phonons. *Nature* 450(7173):1177–1183.
9. Norman MR (2011) The challenge of unconventional superconductivity. *Science* 332(6026): 196–200.
10. Scalapino DJ (2012) A common thread: The pairing interaction for unconventional superconductors. *Rev Mod Phys* 84(4):1383–1417.
11. Davis JC, Lee D-H (2013) Concepts relating magnetic interactions, intertwined electronic orders, and strongly correlated superconductivity. *Proc Natl Acad Sci USA* 110(44):17623–17630.
12. Steglich F, et al. (1979) Superconductivity in the presence of strong Pauli paramagnetism: CeCu2Si2. *Phys Rev Lett* 43(25):1892–1896.
13. Schmidt AR, et al. (2010) Imaging the Fano lattice to 'hidden order' transition in URu_2Si_2. *Nature* 465(7298):570–576.
14. Akbari A, Thalmeier P, Eremin I (2011) Quasiparticle interference in the heavy-fermion superconductor $CeCoIn_5$. *Phys Rev B* 84(13):134505.
15. Allan MP, et al. (2013) Imaging Cooper pairing of heavy fermions in CeCoIn5. *Nature Phys* 9(8):468–473.
16. Petrovic C, et al. (2001) Heavy-fermion superconductivity in CeCoIn5 at 2.3 K. *J Phys Condens Matter* 13(17):L337–L342.
17. Kim JS, Alwood J, Stewart GR, Sarrao JL, Thompson JD (2001) Specific heat in high magnetic fields and non-Fermi-liquid behavior in CeMIn5 (M=Ir, Co). *Phys Rev B* 64(13):134524.
18. Paglione J, et al. (2003) Field-induced quantum critical point in $CeCoIn_5$. *Phys Rev Lett* 91(24):246405.
19. Hu T, et al. (2012) Strong magnetic fluctuations in a superconducting state of $CeCoIn_5$. *Phys Rev Lett* 108(5):056401.
20. Howald L, et al. (2011) Behavior of the quantum critical point and the Fermi-liquid domain in the heavy-fermion superconductor $CeCoIn_5$ studied by resistivity. *J Phys Soc Jpn* 80(2):024710.
21. Paglione J, et al. (2006) Nonvanishing energy scales at the quantum critical point of $CeCoIn_5$. *Phys Rev Lett* 97(10):106606.
22. Bianchi A, Movshovich R, Vekhter I, Pagliuso PG, Sarrao JL (2003) Avoided antiferromagnetic order and quantum critical point in CeCoIn5. *Phys Rev Lett* 91(25):257001.
23. McCollam A, Julian SR, Rourke PMC, Aoki D, Flouquet J (2005) Anomalous de Haas-van Alphen oscillations in $CeCoIn_5$. *Phys Rev Lett* 94(18):186401.
24. Curro NJ, et al. (2012) Anomalous NMR magnetic shifts in $CeCoIn_5$. *Phys Rev B* 64(18): 180514.
25. Kohori Y, et al. (2001) NMR and NQR studies of the heavy fermion superconductors Ce*T*In5 (*T*=Co,Ir). *Phys Rev B* 64(13):134526.
26. Aynajian P, et al. (2012) Visualizing heavy fermions emerging in a quantum critical Kondo lattice. *Nature* 486(7402):201–206.
27. Koitzsch A, et al. (2009) Electronic structure of $CeCoIn_5$ from angle-resolved photoemission spectroscopy. *Phys Rev B* 79(7):075104.
28. Jia X-W, et al. (2011) Growth characterization and Fermi surface of heavy-fermion $CeCoIn_5$ superconductor. *Chin Phys Lett* 28(5):057401.
29. Stockert O, et al. (2011) Magnetically driven superconductivity in CeCu2Si2. *Nature Phys* 7(2):119–124.
30. Izawa K, et al. (2001) Angular position of nodes in the superconducting gap of quasi-2D heavy-fermion superconductor $CeCoIn_5$. *Phys Rev Lett* 87(5):057002.
31. Park WK, Sarrao JL, Thompson JD, Greene LH (2008) Andreev reflection in heavy-fermion superconductors and order parameter symmetry in CeCoIn5. *Phys Rev Lett* 100(17):177001.
32. Ernst S, et al. (2010) Scanning tunneling microscopy studies on $CeCoIn_5$ and $CeIrIn_5$. *Phys Status Solidi* 247(3):624–627.
33. Truncik CJS, et al. (2013) Nodal quasiparticle dynamics in the heavy fermion superconductor $CeCoIn_5$ revealed by precision microwave spectroscopy. *Nat Commun* 4:2477.
34. Zhou BB, et al. (2013) Visualizing nodal heavy fermion superconductivity in $CeCoIn_5$. *Nat Phys* 9(8):474–479.
35. Hanaguri T, et al. (2009) Coherence factors in a high-t_c cuprate probed by quasiparticle scattering off vortices. *Science* 323(5916):923–926.
36. Stock C, Broholm C, Hudis J, Kang HJ, Petrovic C (2008) Spin resonance in the *d*-wave superconductor CeCoIn5. *Phys Rev Lett* 100(8):087001.
37. Yuan T, Figgins J, Morr DK (2012) Hidden order transition in URu_2Si_2: Evidence for the emergence of a coherent Anderson lattice from scanning tunneling spectroscopy. *Phys Rev B* 86(3):035129.
38. Senthil T, Vojta M, Sachdev S (2004) Weak magnetism and non-Fermi liquids near heavy-fermion critical points. *Phys Rev B* 69(3):035111.
39. Flint R, Nevidomskyy AH, Coleman P (2011) Composite pairing in a mixed-valent two-channel Anderson model. *Phys Rev B* 84(6):064514.